

Weighted Delta-Tracking with Scattering

J. S. Rehak^{a,*}, L. M. Kerby^{b,c}, M. D. DeHart^c, R. N. Slaybaugh^a

^a*University of California, Berkeley*

^b*Idaho State University*

^c*Idaho National Lab*

Abstract

In this work, we expand the weighted delta-tracking routine to include a treatment for scattering. The weighted delta-tracking routine adds survival biasing to normal delta-tracking, improving overall problem figure of merit. In the original formulation of this method, only absorption events were considered. We have expanded the method to include scattering, enabling the assessment of three test cases: a pressurized water reactor pin cell, a fast reactor pin cell, and a homogeneous fuel element. We examine the results of these test cases and compare the final figure of merit of infinite flux and total cross-section while incrementally changing the amount of weighted delta-tracking used.

Keywords: Monte Carlo, Neutron transport, Serpent, Delta-tracking, Weighted delta-tracking

1. Introduction

Monte Carlo methods have been used to model neutron transport since first introduced at Los Alamos National Lab by Metropolis and Ulam [9]. Over the last 60 years, the method has been adapted to new computer architectures and expanded to improve the efficiency and accuracy of calculations. The foundation of Monte Carlo simulations is the statistics of simulating repeated events. Therefore, improving the accuracy of results either requires more events or a more efficient use of events. The latter technique, variance reduction, has resulted in brilliant modifications of the Monte Carlo routine over the past few decades.

Many advances have also been made in simulating events more efficiently, speeding up simulations. One such improvement was the introduction of Woodcock delta-tracking [13]. Delta-tracking mitigates some inefficiencies that occur when standard ray tracing is used for complicated geometries or in regions with heavy absorbers. A new method, weighted delta-tracking (WDT) was introduced by Morgan and Kotlyar [8] to combine the delta-tracking routine with survival biasing, a variance reduction technique.

Modern Monte Carlo codes use many efficiency and variance reduction techniques. These allow users to model much larger and more complicated problems

while using less clock time. In many cases, Monte Carlo methods are used alongside deterministic methods. At the Idaho National Lab (INL), researchers are using the Serpent 2 Monte Carlo code [2] to generate multigroup cross-sections for the MOOSE deterministic code. This work is supporting the development of advanced reactors fuels through the restart of the Transient Reactor Test Facility (TREAT) [10].

In this paper, we will begin by providing background discussion about the neutron propagation techniques ray tracing and delta-tracking, and the WDT routine of Morgan and Kotlyar. We will then describe the new work: a novel extension to the WDT that includes scattering. This extension allows us to apply the WDT routine to three test problems using the Serpent 2 Monte Carlo program: a pressurized water reactor (PWR) pin cell, a fast reactor pin cell, and a homogeneous fuel element for the TREAT reactor. We will then examine the results of these simulations and compare them to a base case where the new routine is not used. Finally, we will discuss those results and make a recommendation for the use of WDT in these types of problems.

2. Background

Particle propagation is an integral part of Monte Carlo codes that simulate transport through a medium. In this section, we will discuss two methods to simulate this propagation: ray tracing and Woodcock delta-tracking.

*Corresponding author
Email address: jsrehak@berkeley.edu (J. S. Rehak)

2.1. Ray tracing

The ray tracing method directly follows a particle from collision to collision, assuming that it travels in a straight, statistically-sampled path. Material properties determine the distance between collisions, and therefore material boundaries must be considered explicitly.

Neutrons propagating through a material have an interaction probability characterized by the material's experimentally-determined total cross-section, a value that varies with position and incident neutron energy, $\Sigma_t(\mathbf{r}, E)$. The probability of an interaction occurring in a differential distance ds is related to the macroscopic cross-section:

$$\frac{dP}{ds} = \Sigma_t(\mathbf{r}, E).$$

We assume that each interaction will remove the neutron from the incident flux, as it is absorbed or deflected out of the original path in position, energy, or both. The medium therefore attenuates an incident mono-energetic neutron flux ϕ_0 as a function of distance:

$$\phi(s) = \phi_0 e^{-s\Sigma_t(\mathbf{r})}. \quad (1)$$

The probability that a neutron has its first interaction in differential distance ds after traveling a distance s is found by dividing the flux at that position $\phi(s)$ by the total flux:

$$f(s)ds = \frac{\phi(s)}{\int_0^\infty \phi(s)ds} ds. \quad (2)$$

We consider the cross-section in a region with a single homogeneous material. In this case, the cross-section is no longer a function of position. Therefore, removing the dependence on \mathbf{r} from Eq. (1) and then plugging into Eq. (2), yields [7]:

$$f(s)ds = \Sigma_t e^{-s\Sigma_t} ds. \quad (3)$$

This is the probability density function (PDF) for the distance traveled, s just prior to the first collision. As the distance a neutron travels increases, the value of $f(s)$ decreases exponentially; it is less probable that a neutron will travel further without collision. Integrating from 0 to any value gives the cumulative probability that a collision occurs on that interval. Integrating to an arbitrary position s yields the cumulative distribution function (CDF):

$$F(s) = \int_0^s f(s')ds' = 1 - e^{-s\Sigma_t}. \quad (4)$$

As expected, increasing s causes the probability of any interaction, $F(s)$, to approach unity. As the CDF ranges

from zero to unity, we can sample its value by a uniformly distributed random variable $\xi \in (0, 1]$. The distance is reformulated as function of this sampled random variable:

$$1 - e^{-s(\xi)\Sigma_t} = \xi, \\ s(\xi) = \frac{1}{\Sigma_t} \ln(\xi).$$

After sampling the path length of the neutron, its position is updated based on its original position and direction. We assumed that the cross-section Σ_t was constant in a material region, so the sampled path length is only valid as long as the neutron remains in that region. If the neutron reaches the boundary between two material regions, it must be stopped. There, the remaining propagation distance is calculated for the new material region, and new path lengths sampled. Therefore, each time a path length is sampled, the algorithm must determine the distance to the nearest boundary in the direction of motion. This can become computationally expensive in complicated geometries and when the probability of crossing boundaries with each sample path length is high.

2.2. Woodcock Delta-tracking

As discussed in the previous section, $\Sigma_t(\mathbf{r})$ is a piecewise discontinuous function that varies with position and the geometry of the problem [4]. Using ray tracing, neutrons must stop at these discontinuities to account for the new material region. To avoid the computational inefficiency that this may cause, a rejection sampling technique known as Woodcock delta-tracking was developed [13].

Woodcock delta-tracking introduces a single cross-section to homogenize all the materials in the region of interest. This is chosen to be the maximum of all material total cross-sections, the majorant cross section:

$$\Sigma_{\text{maj}} \equiv \max_{\mathbf{r} \in \mathbf{D}} \{\Sigma_t(\mathbf{r})\}, \quad (5)$$

where \mathbf{D} is the region of interest. The majorant concept is demonstrated in a one-dimensional region in Fig. 1.

As the total cross-section varies in space, we must add a second space-varying function to achieve a constant majorant cross-section:

$$\Sigma_{\text{maj}} = \Sigma_\delta(\mathbf{r}) + \Sigma_t(\mathbf{r}), \quad \forall \mathbf{r} \in \mathbf{D}. \quad (6)$$

To maintain consistency with the physical problem, a delta collision must be interpreted as an event that preserves the neutron's energy and direction. Therefore, we

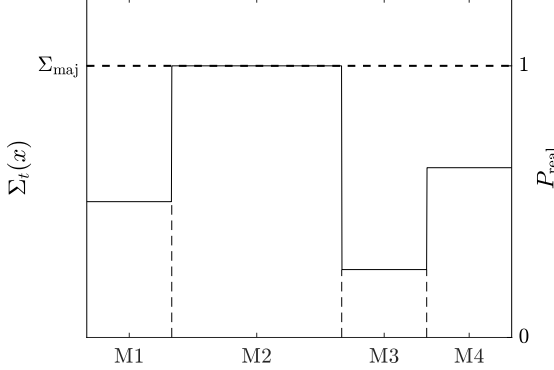


Figure 1: Total cross-section as a function of position. The x -axis is a one-dimensional region of interest divided into four sections M1–M4 with different material properties. The left y-axis shows the total cross-section for each of these material regions, and the chosen majorant cross-section. The right y-axis shows the value of P_{real} over the region.

will refer to these as “virtual” collisions, that can occur any number of times along a neutron’s path without consequence.

The majorant cross-section is constant throughout the entire region of interest, so we can treat it as a single material. Following the same derivation in the previous section, the PDF of the first collision occurring after s in the region of interest using the majorant cross-section is given by:

$$f_{\text{maj}}(s) = \Sigma_{\text{maj}} e^{-\Sigma_{\text{maj}} s} \quad (7)$$

$$= (\Sigma_{\delta}(\mathbf{r}) + \Sigma_t(\mathbf{r})) e^{-\Sigma_{\text{maj}} s}. \quad (8)$$

In most of the region of interest, the majorant cross-section is not the real cross-section and therefore it cannot be used to sample the path length s . Instead, we must use rejection sampling to simulate sampling using the real $\Sigma_t(\mathbf{r})$ while using Σ_{maj} .

As described by Lux and Koblinger [7], rejection sampling requires a PDF of interest, $f(x)$, and a second PDF $g(x)$ for which:

$$f(x) \leq M \cdot g(x), \quad \forall x, \quad (9)$$

where $M \in \mathbf{R}$ is a constant. Sampling from $M \cdot g(x)$ and accepting these samples with probability

$$P = \frac{f(x)}{M \cdot g(x)} \quad (10)$$

replicates sampling directly from $f(x)$.

Using our definition of the majorant cross-section in Eq. (5):

$$\Sigma_{\text{maj}} \equiv \max_{\mathbf{r} \in \mathbb{V}} \{\Sigma_t(\mathbf{r})\} \implies \Sigma_t(\mathbf{r}) \leq \Sigma_{\text{maj}}, \quad \forall \mathbf{r},$$

and therefore

$$\Sigma_t(\mathbf{r}) e^{-s \Sigma_{\text{maj}}} ds \leq \Sigma_{\text{maj}} e^{\Sigma_{\text{maj}} s}, \quad \forall \mathbf{r}.$$

Choosing the left hand side (l.h.s.) to be $f(x)$ and the right hand side (r.h.s.) to be $g(x)$ and $M = 1$ returns the rejection sampling inequality of Eq. (9).

$$f(x) = \Sigma_t(\mathbf{r}) e^{-\Sigma_{\text{maj}} s},$$

$$g(x) = \Sigma_{\text{maj}} e^{-\Sigma_{\text{maj}} s}.$$

Notably, $f(x)$ is the portion of Eq. (8) that represents real collisions. We may therefore sample path lengths using $g(x)$ and accept samples with probability

$$P(\mathbf{r}) = \frac{f(x)}{M \cdot g(x)} = \frac{\Sigma_t(\mathbf{r}) e^{-\Sigma_{\text{maj}} s}}{\Sigma_{\text{maj}} e^{-\Sigma_{\text{maj}} s}} = \frac{\Sigma_t(\mathbf{r})}{\Sigma_{\text{maj}}}, \quad (11)$$

to replicate sampling directly from $f(x)$. If the path length is accepted, it is a real collision and the appropriate routine is executed. Otherwise, it was a virtual collision resulting from the non-physical $\Sigma_{\delta}(\mathbf{r})$ and a new path length is sampled. As pointed out earlier, any number of these can occur. Hereafter, we will refer to $P(\mathbf{r})$ as the probability of a real collision, $P_{\text{real}}(\mathbf{r})$.

It is worth noting that after each path length sample and neutron propagation, the algorithm still requires knowledge of the current material region to lookup $\Sigma_t(\mathbf{r})$ and calculate $P(\mathbf{r})$. The algorithm for delta-tracking is shown in Alg. 1.

Algorithm 1 Delta-tracking

```

1: Sample path length
2: Look up location to get  $\Sigma_t(\mathbf{r})$ 
3:  $P_{\text{real}} \leftarrow \frac{\Sigma_t(\mathbf{r})}{\Sigma_{\text{maj}}}$ 
4: Sample random number  $\xi \in [0, 1)$ 
5: if  $\xi < P_{\text{real}}$  then ▷ Collision is real
6:   Execute real collision
7: else ▷ Collision is virtual
8:   Execute virtual collision
9: end if

```

Now, the path length can be sampled across multiple material regions of varying Σ_t without explicitly stopping the neutron at a given boundary. This allows us

to avoid determining the distance to the nearest boundary after each path length sampling. Therefore, delta-tracking is much more efficient than ray-tracing in regions where the geometry is complex or material region thicknesses are on the same order as the path length. This method can become computationally inefficient in regions where the total cross-section is much less than the majorant cross-section, leading to oversampling of virtual collisions. This is seen in geometries that include localized absorbers, such as control rods.

2.3. Neutron propagation in Serpent 2

The Serpent Monte Carlo code was developed at VTT Technical Research Centre of Finland (VTT) as a PhD thesis project [2]. A second iteration of the code, Serpent 2, is currently under development. Both versions of Serpent use a combination of surface tracking, Woodcock delta-tracking, and rejection sampling for non-uniform density distributions. Serpent 2 selects between surface tracking and delta-tracking by examining the ratio of total cross-section to majorant cross-section [3]. In regions where many virtual collisions would occur, the code preferentially switches to ray tracing. This is to avoid the computational inefficiency of processing virtual collisions that provide no statistics. This selection is determined by a constant c and the following inequality, which is identical to our formulation of P_{real} :

$$\frac{\Sigma_t(\mathbf{r})}{\Sigma_{\text{maj}}} = P_{\text{real}} > 1 - c. \quad (12)$$

If this inequality is true, delta-tracking is used, otherwise ray tracing (referred to as surface-tracking in Serpent 2) is used. By default, the value of c is 0.9, empirically determined to produce the largest improvement in run time [3]. Prior to sampling path length, the code tests this ratio for the current neutron position and determines if surface tracking or delta-tracking should be used. If delta-tracking is used, the code then determines if the collision is virtual or real. The value of c can be changed in the input file using `set dt`.

3. Method

Morgan and Kotlyar [8] introduced a method to improve the inefficiencies of Woodcock delta-tracking in the presence of large absorbers. The method, WDT, replaces the rejection sampling algorithm of delta-tracking with a weight reduction algorithm. This process is a survival biasing technique, like implicit capture.

The WDT method modifies delta-tracking for an absorbing medium, replacing virtual collisions with a

weight reduction. In this chapter, we will discuss the WDT routine for absorption events, and extend the method to include scattering. We will then define the WDT threshold, a key parameter for its implementation in Serpent 2.

3.1. Implicit Statistical Events

We consider a repeatable process that can result in multiple outcomes with independent probabilities. One approach is to sample a random variable and determine which outcome occurs. If the event occurs many times, we can instead replace this process by using the expected value of the process [7]. The expected value of a random variable x that can take values $x_1 \dots x_n$ with probabilities $p_1 \dots p_n$, respectively, is given by:

$$E[x] = x_1 p_1 + x_2 p_2 + \dots + x_n p_n. \quad (13)$$

The expected value provides us with the average value of x if we directly sampled it many times. This method is often applied to neutron propagation in a process called survival biasing [1].

At each collision in an analog simulation, the algorithm samples the type of event to determine the appropriate action. Collision estimators use these collision events to generate the statistics for the simulation. In the case of a capture event, the neutron is killed (removed from the simulation). Capture events that kill neutrons, therefore, are removing the very particles we need to generate better statistics, resulting in the need for many more particles. Mitigating this issue is the goal of survival biasing.

One type of survival biasing is implicit capture, in which capture events are replaced with an expected outcome. As described above, we do not need to track the outcome of every single event, but can rely on the expected value. This will give us, on average, the outcome of our many events. The probabilities p will be given by the ratios of the cross-sections:

$$p_c = \frac{\Sigma_c}{\Sigma_t}, \quad p_s = \frac{\Sigma_s}{\Sigma_t},$$

where Σ_c and Σ_s are the macroscopic cross-sections for capture and scattering, respectively.

We also must introduce the concept of neutron “weight.” All neutrons are born with unity weight and are killed when they have zero weight. This value represents the importance of the neutron, specifically its potential to continue causing collisions. At each point of interaction, the incoming neutron has an initial weight based on the neutron’s history w_i , and a final weight w_f that depends on the type of interaction. A capture event

that kills a neutron immediately forces the final weight of the neutron to zero, $w_{f,c} = 0$. We can then calculate the expected value of the interaction of a neutron with initial weight w_i :

$$E[w_f] = w_{f,s}p_s + w_{f,c}p_c = w_{f,s}p_s$$

A scattering event changes the location of the neutron in energy and angle phase space, leaving its importance unchanged. Therefore, $w_{f,s} = w_i$ and:

$$E[w_f] = w_i p_s. \quad (14)$$

With implicit capture every collision is considered to be a scattering event, and the final weight is set to the expected value of Eq (14). The neutron continues with a lower weight, proportional to the probability that the event was scattering. In effect, discrete capture events are replaced with fractional capture events at each collision.

The weight lost in the collision is scored as capture:

$$\begin{aligned} S_c &= E[w_i - w_f] \\ &= E[w_i] - E[w_f] \\ &= w_i - w_i p_s \\ &= w_i(1 - p_s), \end{aligned}$$

where S_c is the score for capture. A similar method will be used by weighted delta-tracking.

3.2. Russian Roulette

When a survival biasing routine is used, such as the one described in the previous section, the loss of neutrons is entirely reliant on leakage from the problem or fission events. Neutrons will continue to undergo collisions and subsequent weight reduction until they have a very low weight. These particles will only contribute small amounts to the statistics, so tracking these particles is computationally inefficient. To mitigate this, a lower cutoff for the weight is introduced. Once neutrons are below this weight, they have a chance of being killed by a Russian Roulette routine.

The general algorithm is shown in Algorithm 2. Following a collision, if the weight of the colliding particle is below a defined weight threshold, a random number is sampled. If this number is below a defined roulette probability, the particle is killed. If the particle survives roulette, its weight is increased proportionally to the roulette probability. By either killing low weight particles or increasing their weight, the inefficiency of tracking low-weight particles can be reduced.

Algorithm 2 Roulette Routine

```

1: if weight < weight threshold then
2:    $\xi \leftarrow$  random number  $\in [0, 1]$ 
3:   if  $\xi <$  roulette probability then
4:     Kill particle
5:   else
6:      $w_f \leftarrow w_i /$  (roulette probability)
7:   end if
8: end if

```

3.3. Weighted delta-tracking

Morgan and Kotlyar [8] introduced a method to improve the inefficiencies of Woodcock delta-tracking in the presence of large absorbers. The method, WDT, replaces the rejection sampling of delta-tracking with a weight reduction. This is a survival biasing process, similar to implicit capture discussed in Section 3.1.

The WDT method samples the particle path length in the same fashion as Woodcock delta-tracking. As described in Section 2.2, after each path length is sampled, the delta-tracking method accepts the collision as real with the probability shown in Eq. 10. The WDT method bypasses this rejection sampling by accepting all collisions as real with a subsequent reduction in weight. As discussed in Section 3.1, replacing a statistical event requires calculation of the expected value. In this case, the two events are a real collision and a virtual collision:

$$E[w_f] = w_{f,\text{real}}P_{\text{real}} + w_{f,\text{virt}}P_{\text{virt}}. \quad (15)$$

Morgan and Kotlyar examine a 1D test case with absorption. As an absorption event removes the particle, the resulting final weight of a real collision is zero. A virtual collision is rejected, and therefore leaves the weight unchanged. Inserting the appropriate values into Eq. (15) gives the expected value of the final weight for an absorption event:

$$\begin{aligned} E[w_f] &= w_{f,\text{real}}P_{\text{real}} + w_{f,\text{virt}}P_{\text{virt}} \\ &= 0 + w_i P_{\text{virt}} \\ &= w_i(1 - P_{\text{real}}) \\ &= w_i \left(1 - \frac{\Sigma_t}{\Sigma_{\text{maj}}}\right). \end{aligned}$$

The particle that is left following the collision continues propagating as if it underwent a virtual collision. In this case, the absorption is then scored using the expectation

value of the score.

$$\begin{aligned} S_{\text{absorption}} &= E[w_i - w_f] \\ &= E[w_i] - E[w_f] \\ &= w_i \left(\frac{\Sigma_t}{\Sigma_{\text{maj}}} \right) \end{aligned}$$

This algorithm is implemented by Kotlyar and Morgan in a 1D problem and the results are verified with an analytical solution. The authors point out that a rouletting routine should be implemented when WDT is used, to prevent the tracking of low-weight neutrons.

3.4. Weighted delta-tracking with scattering

In a scattering event, the weight of the incident particle does not change. Therefore, application of the expectation value as in the previous section results in an expected value of the final weight equal to the initial weight:

$$\begin{aligned} E[w_f] &= w_{f,\text{real}} P_{\text{real}} + w_{f,\text{virt}} P_{\text{virt}} \\ &= w_i P_{\text{real}} + w_i P_{\text{virt}} \\ &= w_i (P_{\text{real}} + 1 - P_{\text{real}}) \\ &= w_i. \end{aligned}$$

This doesn't model what we expect. We can view WDT as splitting the weighted neutron into two particles. One carries the real portion of the weight and experiences the collision. The other carries the virtual portion of the weight and continues propagating as if no collision occurred. This works for absorption, where the portion that experiences the collision does not propagate: it is immediately killed and scored. But, when the neutron is split into a scattering portion and a virtual portion, no weight is lost because neither of those events change the weight.

Therefore, extension of this methodology to scattering requires duplication of the particle at the point of collision. The virtual portion of the weight is carried away by a particle that propagates as if no collision has occurred, and the real portion is carried away by a particle that undergoes scattering. In problems with scattering, this results in a rapid multiplication of neutrons. When implemented into Serpent 2, this multiplication very quickly filled any available neutron buffer in simulations of a boiling water reactor (BWR), ending the simulation.

To address this issue, we expanded the WDT method with a novel approach to handling scattering. This approach combines the WDT methodology with the standard delta-tracking rejection sampling in a way that has not been done before.

3.5. Scattering Rejection Sampling

As described in the last section, the WDT method may result in an intractable simulation when applied to scattering. This occurred because the WDT method splits the incoming weight in two: one portion for a real collision, one portion for a virtual collision. We developed a new methodology that avoids splitting the neutron when scattering, while keeping the splitting otherwise. To accomplish this, the original delta-tracking rejection sampling was moved into the scattering subroutine. The algorithm is shown in Alg. 3 and a flow chart of the routine is shown in Fig. 2.

Note that there are two separate scoring events in each collision subroutine: scoring of the actual collision type for calculating specific reaction rates, and scoring of collision itself used by the collision flux estimator. In addition, scoring the fission reaction also encompasses generation of fission neutrons.

In the original delta-tracking routine, the rejection sampling takes place prior to collision type sampling, and collision scoring can occur between the two. This is the routine that Serpent 2 generally uses; for this study, we used a Serpent 2 source code modified to implement the above scheme. By moving the rejection sampling after the collision type sampling, the collision score is no longer agnostic to the type of collision that will occur. Therefore, in the implementation of this routine in Serpent 2, the collision scoring was moved after the collision type sampling.

This method is a survival biasing method, like implicit capture, as capture events no longer remove neutrons from the simulation. The WDT routine differs from implicit capture in the cross-sections used to reduce the weight. Implicit capture uses the ratio of the capture to the total cross-sections, while WDT uses the ratio of the total to the majorant cross-sections.

3.6. Implementation in Serpent 2

The WDT algorithm is implemented to work alongside the current implementation of ray tracing and delta-tracking. WDT is designed to improve the effectiveness of delta-tracking when the change of a virtual collision is high. We can hypothesize that the algorithm will benefit in the regime where P_{real} is low. At high values of P_{real} , a majority of the weight of the incoming particle is scored. This leaves the particle that undergoes a virtual collision with a very low weight, relying on the rouletting routine to prevent computational inefficiency. These two situations imply that there is a region between low and high values of P_{real} where WDT may provide benefit.

This region is defined by two values, summarized in Fig. 3. On the lower end, the value of $(1 - c)$ defines

Algorithm 3 Weighted delta-tracking with scattering

```

1: Sample path length
2: Sample collision type
3: if collision type == (capture or fission) then
4:   Score capture or fission  $\leftarrow w_i P_{\text{real}}$ 
5:   Score collision  $\leftarrow w_i P_{\text{real}}$ 
6:    $w_f \leftarrow w_i(1 - P_{\text{real}})$ 
7:   Execute virtual collision
8: else
9:   Sample random number  $\xi \in [0, 1]$ 
10:  if  $\xi < P_{\text{real}}$  then  $\triangleright$  Collision is real
11:    Score scattering  $\leftarrow w_i$ 
12:    Score collision  $\leftarrow w_i$ 
13:    Execute scattering collision
14:  else  $\triangleright$  Collision is virtual
15:    Execute virtual collision
16:  end if
17: end if

```

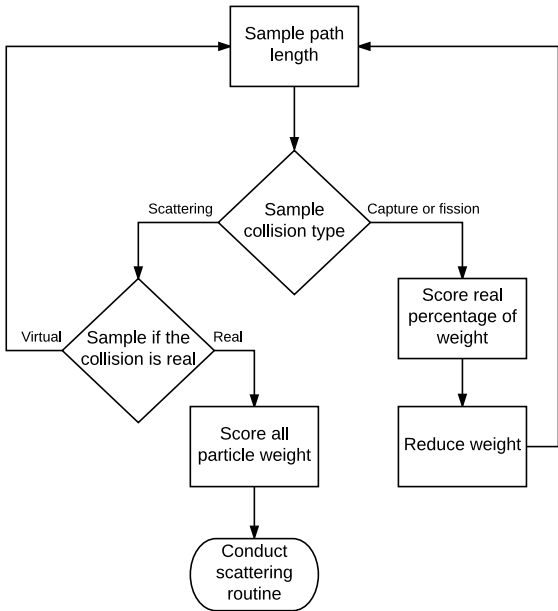


Figure 2: Weighted delta-tracking with scattering rejection sampling.

the threshold below which surface tracking is used. On the upper end, a new parameter t_{wdt} defines the threshold below which WDT will be used instead of normal delta-tracking. This provides the user with the ability to exactly define the region where WDT will be used using the following relationship,

$$\text{Mode} = \begin{cases} \text{Ray tracing,} & P_{\text{real}} < 1 - c \\ \text{WDT,} & 1 - c \leq P_{\text{real}} < t_{\text{wdt}} \\ \text{Delta-tracking,} & P_{\text{real}} \geq t_{\text{wdt}} . \end{cases}$$

4. Results

We expect that the WDT method will improve the statistics of Serpent calculations. With normal delta-tracking, virtual collisions provide no statistical benefit, and are therefore an inefficient use of computational resources. Virtual collisions that result in absorption events do contribute to statistics when using WDT. Therefore, we expect an improvement in the results of a Serpent 2 simulation. In this section, we describe how we quantify performance in this study, three test cases, and the results of those test cases.

4.1. Figure of Merit

Monte Carlo codes such as Serpent 2 run many iterations of a single simulation, calculating the mean of values of interest \hat{x} across many runs. All calculations done in this study were criticality source calculations. For these types of calculations in Serpent 2, source neutrons are run in cycles. Each cycle contains the same number of source neutrons, and the source distribution is determined by the previous cycle [5]. By the central limit theorem, we know that the means across these many simulations will form a normal distribution with variance $\sigma^2(\hat{x})$. We are interested in reducing the variance of the final value, which will provide more confidence in the simulation results. In general, running the simulation more times with more particle histories will reduce this variance at the cost of requiring more computation time. The variance depends on the number of particle histories, which is proportional to the number of cycles n :

$$\sigma^2(\hat{x}) \propto \frac{1}{n} . \quad (16)$$

Cycles will be used in the place of particle histories because this value is easily drawn from the Serpent 2 output files.

Serpent 2 reports the relative error of the mean [11], $\sigma(\hat{x})$, which is proportional to $n^{-1/2}$. Per the central limit theorem and Eq. (16), we can always continue running

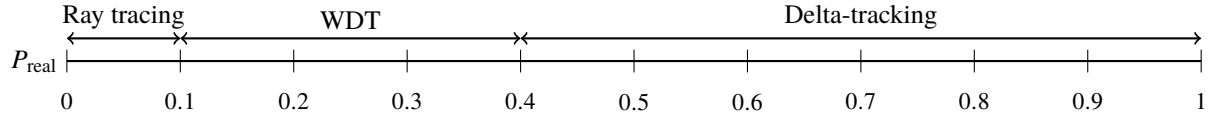


Figure 3: Implemented selection scheme for ray-tracing, weighted, and normal delta-tracking. Shown using the values of $(1 - c) = 0.1$ and $t_{\text{wtd}} = 0.4$.

more cycles to improve the variance. A more efficient simulation should provide better statistics, resulting in a lower variance in less time. The variance is therefore dependent on two things: the number of cycles we run, and the efficiency of our algorithm.

For this study, we are interested in the efficiency of the WDT algorithm. We therefore need to establish a standard measuring device, a figure of merit (FOM), that is independent of the number of cycles, n . This will then allow us to utilize the variance to directly measure of the efficiency of our algorithm. The standard FOM described by Lewis and Miller [1], is

$$\text{FOM} = \frac{1}{\sigma(\hat{x})^2 T}, \quad (17)$$

where T is the runtime of the simulation and is proportional to the number of cycles $T \propto n$. Plugging this and Eq. (16) into Eq. (17) yields:

$$\text{FOM} = \frac{1}{\sigma(\hat{x})^2 T} = \frac{n}{C_1} \cdot \frac{1}{C_2 \cdot n} = C_3,$$

where C_1, C_2, C_3 are constants.

As we can see, we expect the FOM to be a constant value, independent of the number of cycles n . A higher FOM indicates higher accuracy per computation time, and therefore a more efficient algorithm. In practice, this constant is still a statistical quantity. Therefore, many cycles are required until enough statistics are collected to calculate the mean and variance of the FOM.

An accurate comparison of FOM requires that all the simulations are run with identical computer loading. To ensure that the loading does not change throughout the simulation, we calculated the number of cycles completed per CPU time and ensured that it was a constant value. A constant cycles/CPU time does not ensure that the loading is the same for all simulations, only that it did not change during that simulation's run. To ensure that our FOM values could be accurately compared, we calculated the value in two steps.

First, all simulations were run for a long enough period for the FOM to converge. The cycles/CPU time is observed to ensure computer loading did not change.

Then, the FOM at each point in the simulation is calculated using the total *cycles*, C :

$$\text{FOM}_C = \frac{1}{\sigma(\hat{x})^2 C}. \quad (18)$$

Then all connections were isolated to the cluster so that no other loading would be placed on it. We ran each of the simulations for a shorter duration (approximately two hours) to ensure a value of cycles/CPU time converges. This is then multiplied by FOM_C to return the FOM:

$$\text{FOM}_C \cdot \frac{C}{T} = \frac{1}{\sigma(\hat{x})^2 C} \cdot \frac{C}{T} = \frac{1}{\sigma(\hat{x})^2 T} = \text{FOM}. \quad (19)$$

This process ensures that the FOM for all runs is normalized to the same computer loading.

4.2. Analysis Package

As discussed in the previous section, we want to observe the convergence behavior of the FOM to determine the final value. To do so, we modified the Serpent 2 source code to generate uniquely named output files at various cycle values. We developed the `WDT_Analysis` package¹ to leverage python's object oriented programming structure and enable easy analysis of the data. We utilize a module, `fom`, to analyze the convergence of FOM across many Serpent 2 output files.

4.3. Parameters of study

Each Serpent 2 simulation generates hundreds of output parameters that describe all processes that occur during particle propagation. To focus our search, we identified two quantities that will be the focus of this study: flux and total cross-section. Further study into other parameters may reveal further benefit or issues with the WDT method. Each of the three test cases have reflective boundary conditions, so we will examine the infinite values for the parameters of interest.

A Serpent 2 simulation was run for each test case using values of the WDT threshold (t_{wtd}) from 0.1 to unity in

¹Available on GitHub https://github.com/jsrehak/WDT_Analysis

increments of 0.1, maintaining a constant threshold to ray tracing (surface tracking) as described in Fig. 3. To determine the effectiveness of WDT, we normalized the final FOM for each value of t_{wdt} to the final FOM with no WDT:

$$\text{FOM}_{\text{norm}}(t_{\text{wdt}}) = \frac{\text{FOM}(t_{\text{wdt}})}{\text{FOM}_0},$$

where $\text{FOM}_0 = \text{FOM}(0.1)$ is the FOM with no WDT. Increasing values of t_{wdt} leads to increasing the amount of WDT over regular delta-tracking. The parameters for the roulette scheme are kept constant, with a weight cutoff of $w = 0.1$ and probability of roulette $P_{\text{kill}} = 0.5$.

Three test cases were selected to test the performance of the WDT method. These are a PWR pin cell, a fast reactor pin cell, and a homogenous fuel element based on the composition of the TREAT fuel elements at the INL. We chose the PWR pin cell to evaluate the WDT algorithm when energy domains are dominated by either scattering (fast) or absorption (thermal). The fast reactor pin cell provides a contrasting situation where both scattering and absorption occur in the fast group. Finally, the TREAT fuel element was chosen to assess the ability of WDT to improve overall cross-section generation for deterministic codes. All test cases were run on a small cluster at the University of California, Berkeley, and the specifications of the cluster are shown in Tab. 1.

4.4. Pressurized water reactor pin cell

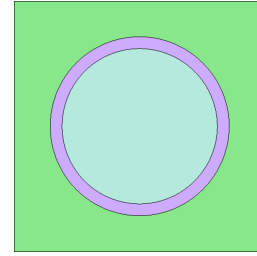
The PWR pin cell was chosen from the Serpent 2 validation input files provided on the VTT Serpent webpage [12]. The geometry and physical parameters are shown in Fig. 4. The fuel is a 2.68 w/o enriched UO_2 mixture, with Zircalloy cladding, light water moderation, and reflective boundary conditions. We ran the simulation with two energy groups with the group boundary at 0.625 eV.

The cycles/CPU time (C/T) for each value of t_{wdt} are shown in Fig. 5 and the raw data are included in Appendix A in Table A.4. We note, looking at the graph, that the cycles/CPU time initially decreases linearly as more WDT is applied, and then reaches a constant value when $t_{\text{wdt}} = 0.4$.

4.4.1. PWR infinite flux

For the PWR pin cell infinite flux (ϕ_{∞}), the FOM of the fast and thermal groups are shown in Fig. 6. The data in this graph are included in Appendix A in Table A.5.

We see a general improvement in the flux FOM for all but one value (the fast flux when $t_{\text{wdt}} = 0.3$). We expect



Parameter	Value (cm)
Fuel radius	0.412
Cladding radius	0.475
Pitch	1.33

Figure 4: Pressurized water reactor geometry and physical parameters. The fuel is shown in light blue, the cladding in purple and the coolant is green.

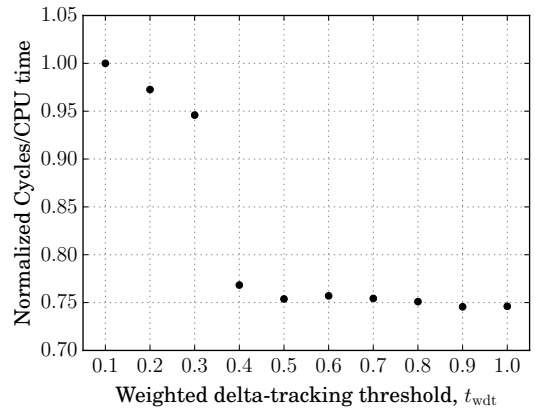


Figure 5: Cycles/CPU time for the PWR pin cell for the range of t_{wdt} studied. Values are normalized to the base case without WDT.

Table 1: Small cluster specifications

Parameter	Specification
Processor	2 × TenCore Intel Xeon Processor E5–2687W v3 3.10 GHz 25MB Cache
RAM	16 × 16GB PC4–17000 2133MHz DDR4
Hard drive	2 × 800 GB Intel SATA 6.0 GB/s Solid State Drive

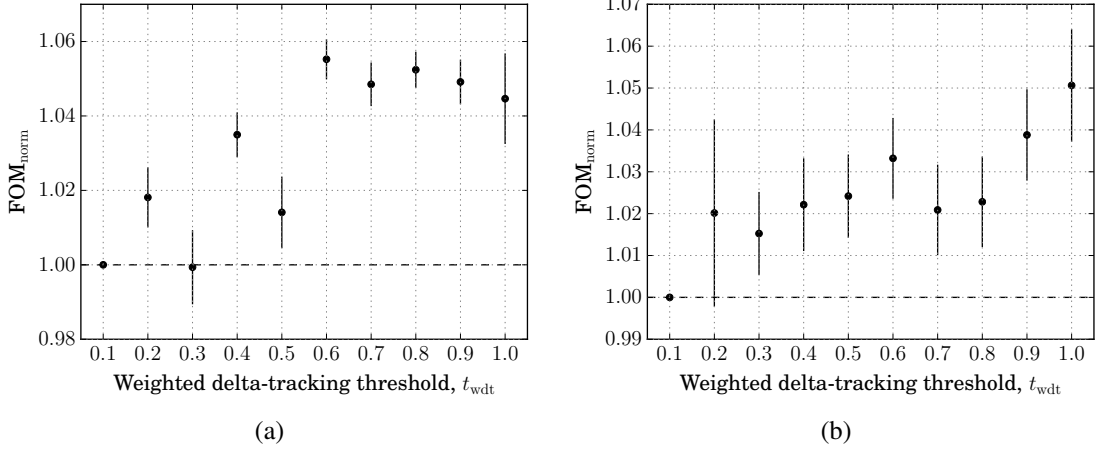


Figure 6: FOM for the PWR infinite flux ϕ_∞ for the (a) fast and (b) thermal groups. Error bars shown are one standard deviation.

the FOM to improve, as the WDT method with scattering introduces survival biasing by replacing absorption events with a weight reduction, as discussed in Sec. 3.1. In this case, the improvement in FOM shows that the variance reduction introduced by WDT is greater than the reduction in computation efficiency that we noted in Sec. 4.4. The magnitude of improvement in the fast flux increases before leveling out when $t_{\text{wdt}} = 0.6$.

4.4.2. PWR infinite total cross-section

For the PWR pin cell infinite total cross-section ($\Sigma_{t,\infty}$), the FOM of the fast and thermal groups are shown in Fig. 7. The data in this graph are included in Appendix A in Table A.6. For the fast flux, WDT clearly underperforms the base case, following the graph of cycles/CPU time very closely. For the thermal group, an overall improvement is noted for all but one value of t_{wdt} .

4.5. Fast reactor pin cell

We adapted the fast reactor pin cell from another example provided in the Serpent validation files [12]. This is a lead cooled pin cell with Mixed Oxide (MOX) fuel containing uranium, plutonium and a small amount of americium. The relative isotope amounts are shown in Tab. 2. The cladding is stainless steel, and the lattice is hexagonal with reflective boundary conditions. As with

the PWR pin cell, we ran the simulation with two energy groups with the group boundary at 0.625 eV.

Table 2: Relative atomic density of the fast reactor pin cell MOX fuel.

Isotope	Relative Atomic Density
^{238}U	1.00
^{239}Pu	0.16
^{240}Pu	7.40×10^{-2}
^{242}Pu	2.09×10^{-2}
^{238}Pu	6.45×10^{-3}
^{235}U	4.11×10^{-3}
^{241}Am	3.57×10^{-3}
^{236}U	1.00×10^{-4}
^{234}U	3.01×10^{-5}

The cycles/CPU time (C/T) for each value of t_{wdt} are shown in Fig. 9 and the raw data are included in Appendix B in Table B.7. There is a clear trend in the cycles/CPU time as the amount of WDT increases. We note that the efficiency of the algorithm falls off more slowly than in the case of the PWR.

4.5.1. Fast reactor infinite flux and total cross-section

For the fast pin cell, the FOM of the fast group for the infinite flux and total cross-section are shown in Fig. 10.

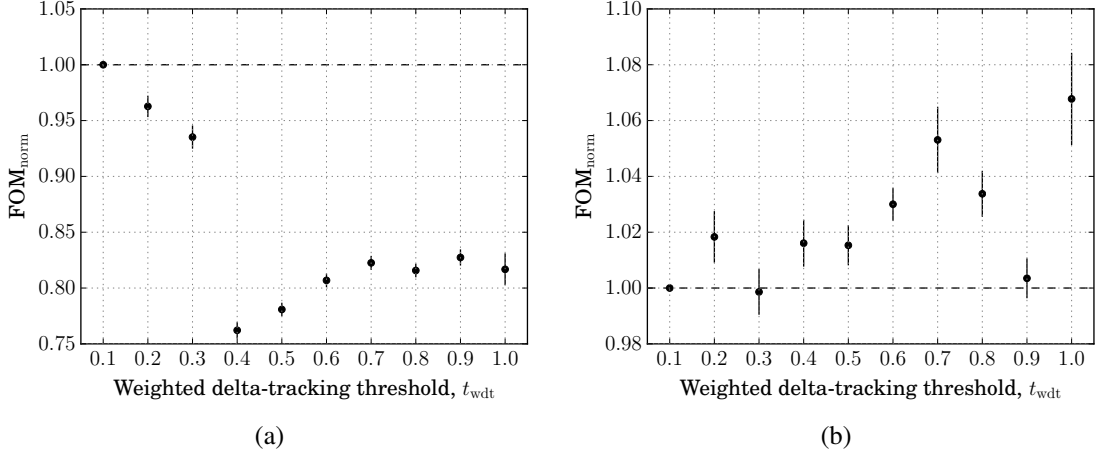
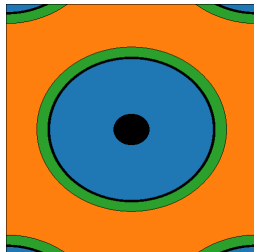


Figure 7: FOM for the PWR infinite total cross-section $\Sigma_{t,\infty}$ for the (a) fast and (b) thermal groups. Error bars shown are one standard deviation.



Parameter	Value (cm)
Void radius	0.1
Pellet radius	0.45
Inner cladding radius	0.465
Outer cladding radius	0.525
Pitch	1.789

Figure 8: Fast pin cell geometry and physical parameters. The pellet is shown in blue, the cladding green, and the coolant orange. Black regions are voids.

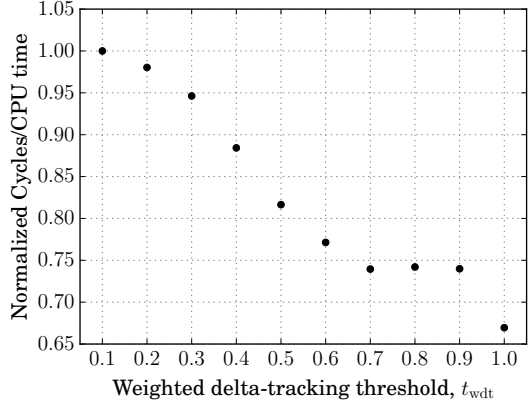


Figure 9: Cycles/CPU time for the fast reactor pin cell for the range of $t_{w\text{dt}}$ studied. Values are normalized to the base case without WDT.

The FOM for the thermal group is not shown, as the relative errors associated with the results were too poor to calculate meaningful FOM values.

We note a similar pattern in the fast infinite flux and total cross-section. There is an overall improvement until a threshold value of $t_{w\text{dt}} = 0.6$ and then a drop. The improvement in FOM is much higher than in the PWR, with improvements at $t_{w\text{dt}} = 0.6$ of $33.5 \pm 1.8\%$ for infinite flux and $19.8 \pm 2.3\%$ for infinite total cross-section.

4.6. Homogeneous fuel Element

The third test case is derived from the TREAT reactor at INL. Work at INL focuses on using deterministic solvers to model the core; the Serpent 2 Monte Carlo code is used to generate the cross-sections for these solvers. We used a homogenized fuel element that

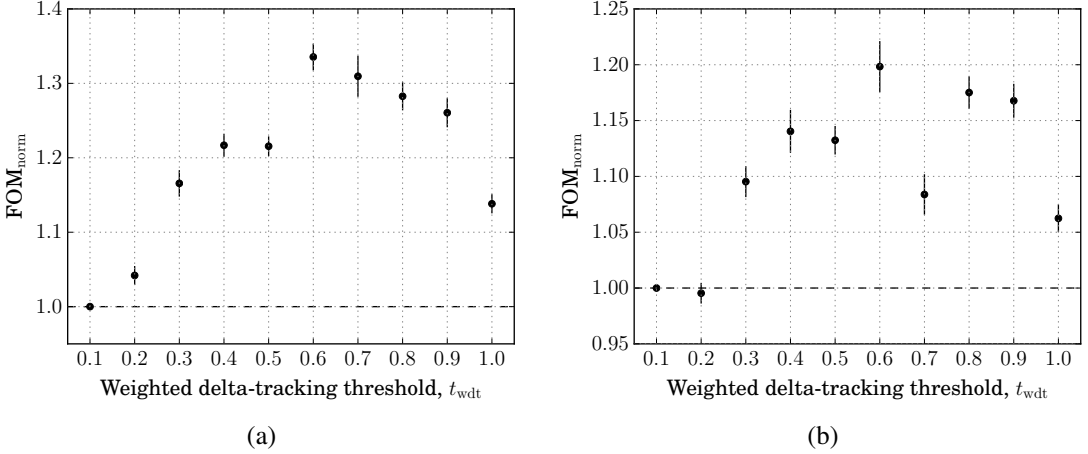


Figure 10: FOM for the fast pin cell infinite (a) flux ϕ_{∞} and (b) total cross-section $\Sigma_{t,\infty}$ for the fast group. Error bars shown are one standard deviation.

replicates the material but not geometry of the TREAT fuel. The simulation uses eleven energy groups, which replicates the groups used by the deterministic solvers. This group structure is summarized in Table 3.

To simplify the analysis, and to allow comparison between the other two test cases, these groups can be collapsed. We can sum all the ϕ_{∞} for each energy group to get a total ϕ_{∞} for the entire energy range. As there is no covariance, the variance of the sum will be the sum of the variance [6]. The variance for summing energy groups g to g' is therefore:

$$\text{Var} \left(\sum_{j=g}^{g'} \phi_{g,\infty} \right) = \sum_{j=g}^{g'} \text{Var} (\phi_{g,\infty}) .$$

This allows us to collapse groups one through six into a fast group, and groups seven through eleven into a thermal group. The boundary of group seven aligns with the separation of the two groups in the previous test problems, so we can compare the results in a more natural fashion.

The cycles/CPU time for each value of t_{wtd} are shown in Fig. 11 and the raw data are included in Appendix C in Table C.9. For all values of t_{wtd} there is little deviation from the base case, with a maximum deviation of 0.19% when $t_{\text{wtd}} = 0.9$. Therefore, unlike with the PWR pin cell and the fast reactor pin cell, increased usage of the WDT routine does not have an impact on computational efficiency. Any large change in FOM will therefore result from a reduction in variance.

4.6.1. Homogeneous infinite flux

For the homogeneous fuel element infinite flux (ϕ_{∞}), the FOM of the fast and thermal groups are shown in

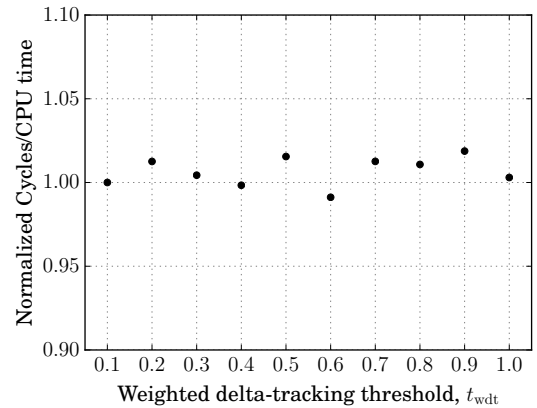


Figure 11: Cycles/CPU time for the homogenous fuel element for the range of t_{wtd} studied. Values are normalized to the base case without WDT.

Fig. 12. The data in this graph are included in Appendix C in Table C.10.

The WDT method shows improvement for both the fast and thermal ϕ_{∞} for values of $t_{\text{wtd}} = 0.4, 0.5$. For both energy groups, the improvement is meager, with a maximum improvement of 6.2% for the fast group and 3.2% for the thermal group. Outside of those values, there is no clear trend or correlation between FOM and the value of t_{wtd} . The homogeneous fuel element is a scattering-dominated system at all energies, so this may be mitigating any variance reduction provided by the survival biasing in WDT

Table 3: Energy group structure for the homogenous fuel element.

Group	Upper energy limit (MeV)	Group	Upper energy limit (MeV)
1	20.0000	7	6.25000×10^{-7}
2	3.32870	8	2.09610×10^{-7}
3	1.15620×10^{-1}	9	7.64970×10^{-8}
4	3.48110×10^{-3}	10	4.73020×10^{-8}
5	1.32700×10^{-4}	11	2.00100×10^{-8}
6	8.10003×10^{-6}		

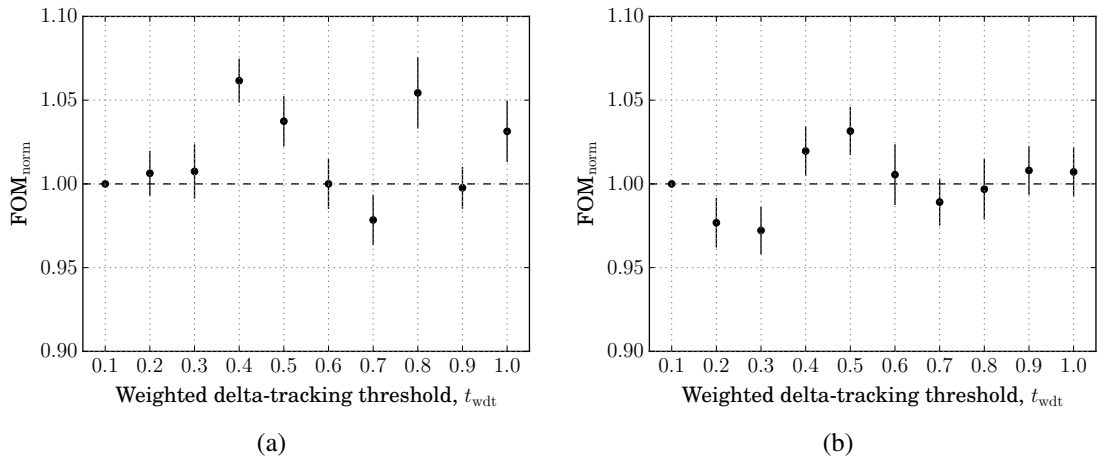


Figure 12: FOM for the homogeneous fuel element infinite flux ϕ_∞ for the (a) fast and (b) thermal group. Error bars shown are one standard deviation.

4.6.2. Homogeneous infinite total cross-section

For the homogeneous fuel element infinite total cross-section ($\Sigma_{t,\infty}$), the FOM of the fast and thermal groups are shown in Fig. 13. The data in this graph are included in Appendix C in Table C.11.

The normalized FOM for the total cross-section for the fast group appears to vary randomly about unity. There is no clear pattern to the values, so the variation may be only due to the stochastic nature of the FOM. For the thermal group, WDT under-performs except when $t_{\text{wdt}} = 0.7, 0.8, 1.0$. In these cases, the largest improvement is for $t_{\text{wdt}} = 0.7$, with an increase in FOM of $5 \pm 2\%$.

5. Discussion

In the previous section, we summarized the results of three test cases: a PWR pin cell, a fast reactor pin cell, and an homogeneous fuel element. We varied the WDT threshold value (t_{wdt}) and calculated the resulting FOM value after convergence. In addition, we presented the computational efficiency, which contributes to the FOM, by calculating the total cycles per unit CPU time over the course of the simulation.

As we described in Section 3.4, the WDT routine with scattering re-inserts the rejection sampling of delta-tracking into the scattering branch decision tree. With standard delta-tracking, virtual collisions do not sample the type of collision. In WDT with scattering, the type of collision is sampled first, so virtual collisions *do* sample the type of collision. This extra sampling in the decision tree results in lower computational efficiency in test problems with more virtual collisions.

We see the effects of this in the cycles/CPU plots for the PWR pin cell and the fast reactor pin cell, Figures 5 and 9, respectively. The computational efficiency suffers when WDT is introduced, and in both cases shows a plateau behavior at 75% of the delta-tracking efficiency. In the base delta-tracking case, the average number of virtual collisions per history in the fast reactor is 40.6, while in the PWR it is 99.0. The higher number of virtual collisions in the PWR causes a steeper drop-off in the computational efficiency in that simulation.

This reduction in efficiency is not seen in the homogeneous fuel element, where the simulation has no virtual collisions. The entire element is a single material region, so at all points the probability of a real collision is unity.

For the FOM, we expect domains with more scattering to perform more poorly, as the scattering decision tree has an extra sample. In contrast, regions with more absorption should see an improvement, due to the introduction of survival biasing.

5.1. Infinite flux

For both the PWR and the fast reactor pin cells, we observe an improvement in the fast group infinite flux as more WDT is introduced. The improvement in both cases reaches a maximum value at $t_{\text{wdt}} = 0.6$ and then declines, slightly in the PWR case and more quickly in the fast reactor case. In addition, the improvement relative to the base case for the fast reactor is much larger than for the PWR. This may be because all the absorption in the fast reactor takes place in the fast group, and therefore the benefits of the survival biasing are more apparent. For the thermal group, the survival biasing results in a clear linear trend in the FOM values.

For the homogeneous fuel element, the FOM for both groups does not appear to follow a trend. The improvement may be due to the stochastic nature of the FOM.

5.2. Infinite total cross-section

For the PWR fast group infinite total cross-section, the normalized FOM looks very similar to the cycles/CPU time data in Fig. 5. This indicates that in this regime, the inefficiency in computation time introduced by WDT is a larger effect than any improvement in variance reduction. The cycles/CPU time is also expected to be constant, while the variance is a statistical quantity. Thus, as a more constant effect is dominating the FOM, the standard deviation of the FOM is much smaller. Despite the introduction of survival biasing, the dominance of scattering reactions in this regime is probably the cause of this.

This trend is contrasted with the fast reactor pin cell, where we see an overall improvement in the FOM for the total cross-section at all values. In this test problem, the absorption occurs in the fast group so the FOM is improved by survival biasing. We hypothesize that the survival biasing effect of the WDT is eventually overcome by the reduction in efficiency at higher values of t_{wdt} .

For the thermal region of the PWR pin cell, there is a clear rise ***in what?*** with increasing t_{wdt} before falling again. Overall improvement is seen at all values of $t_{\text{wdt}} \neq 0.3$. Further investigation into values of t_{wdt} in the vicinity of 0.9 should reveal if there is an overall increasing trend with 0.9 as the outlier, or if the FOM value at 1.0 is the outlier.

5.3. Threshold values

Based on the data collected in this parameter study, we can make some recommendations for the use of WDT with scattering. We anticipate that the lessons learned in the tested physics regimes will translate to problems

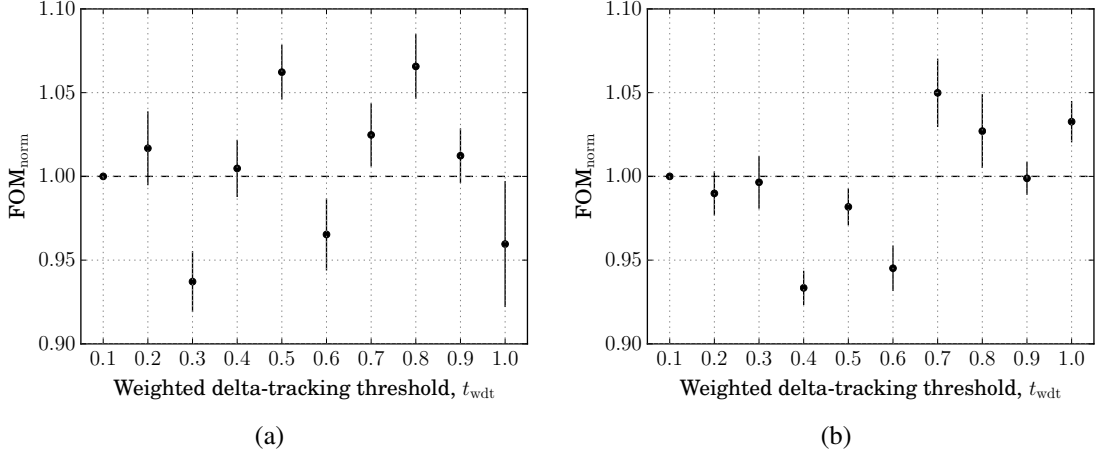


Figure 13: FOM for the homogeneous fuel element infinite total cross-section $\Sigma_{t,\infty}$ for the (a) fast and (b) thermal group. Error bars shown are one standard deviation.

with similar features. Further study is needed to assess if there is improvement in other parameters in these and other types of cases. In addition, these recommendations are based on a comparison to the analog base case.

Based on the data collected here, for a PWR pin cell, a value of t_{wtd} of unity should be chosen, replacing all delta-tracking with WDT. As discussed previously, the large number of virtual collisions causes introduction of any WDT to reduce overall efficiency rapidly. Therefore, the most WDT should be used to leverage as much survival biasing as possible. If very high accuracy in the fast group cross-section is desired, no WDT should be used, as this resulted in a reduction in FOM that is more significant than the improvements in the other parameters.

For a fast reactor pin cell, there appears to be a tipping point beyond which the introduction of more WDT reduces overall efficiency. A value of t_{wtd} of 0.6 should be chosen to maximize the overall improvement in flux and total cross-section.

For the homogeneous fuel element, we can not make a good recommendation for a value of t_{wtd} . Use of WDT does not change the FOM to a large enough degree to overcome the expected statistical fluctuations in calculated FOM.

6. Conclusion

In this work, we described the techniques used by Monte Carlo codes for neutron propagation, including ray-tracing and delta-tracking. We described the WDT method and a novel extension of the method to include scattering. We implemented the method in the Serpent

2 Monte Carlo code and examined the results of simulations with three test cases. We compared the FOM for two simulation results against the base case to determine the best value of the t_{wtd} parameter that defines how much WDT is used in the simulation.

Based on these results, we can conclude that the WDT routine with scattering does improve FOM in infinite flux for the PWR and fast reactor pin cells. For total cross-section, FOM is similarly improved, except in the fast group for the PWR pin cell. We hypothesize that the main driver in improving FOM increased use of survival biasing as more WDT is used, compared to the overall reduction in efficiency in using the routine. In problem domains where scattering is dominant, the increased inefficiency of the routine becomes the driving force, as in the fast group of the PWR. In addition, we confirmed that the inefficiency of the WDT routine has a higher impact on problems that have more virtual collisions.

There is no data to suggest that the WDT results in a statistically significant change in the FOM of those quantities for the homogeneous fuel element. The method was just as efficient as regular delta-tracking, as this test case has no virtual collisions.

It is evident that the survival biasing introduced by WDT is the dominant factor in domains where absorption occurs. Further study should be done to compare the use of WDT with scattering to problems where other types of survival biasing, such as implicit capture, are used, contrasted to this study where the base case used analog Monte Carlo. In addition, a finer resolution in values of t_{wtd} will provide clearer relationships between the amount of WDT and any improvement in FOM

7. Acknowledgments

This research was prepared under award NRC-HQ-84-14-G-0042 from the Nuclear Regulatory Commission. The statements, finding, conclusions, and recommendations are those of the author(s) and do not necessarily reflect the view of the US Nuclear Regulatory Commission. This work was also supported in part by the U.S. Department of Energy, Office of Nuclear Energy, Advanced Modeling and Simulation Program, under DOE- NE Idaho Operations Office Contract DEAC07-05ID14517.

References

- [1] E. E. Lewis and W.F. Miller, Jr. *Computational Methods of Neutron Transport*. American Nuclear Society, 1993.
- [2] J. Leppänen. *Development of a New Monte Carlo Reactor Physics Code*. PhD thesis, Helsinki University of Technology, 2007.
- [3] Jaakko Leppänen. Performance of Woodcock delta-tracking in lattice physics applications using the Serpent Monte Carlo reactor physics burnup calculation code. *Annals of Nuclear Energy*, 37:715–722, 2010.
- [4] Jaakko Leppänen. Modeling of Nonuniform Density Distributions in the Serpent 2 Monte Carlo Code. *Nuclear Science and Engineering*, 174:318–325, 2013.
- [5] Jaakko Leppänen. *Serpent – A Continuous-energy Monte Carlo Reactor Physics Burnup Calculation Code – User’s Manual*, June 2015.
- [6] John. R. Taylor. *An Introduction to Error Analysis*. University Science Books, Second edition, 1997.
- [7] Iván Lux and László Koblinger. *Monte Carlo Particle Transport Methods: Neutron and Photon Calculations*. CRC Press, 1991.
- [8] L.W.G. Morgan and D. Kotlyar. Weighted-delta-tracking for Monte Carlo particle transport. *Annals of Nuclear Energy*, 85:1184–1188, 2015.
- [9] N. Metropolis and S. Ulam. The Monte Carlo Method. *Journal of the American Statistical Association*, 44(247):335–341, 1949.
- [10] J. Ortensi et al. Updates to the Generation of Physics Data Inputs for MAMMOTH Simulations of the Transient Reactor Test Facility. Technical Report INL/EXT-16-39120, Idaho National Laboratory, June 2016.
- [11] Toni Kaltiaisenaho. Statistical Tests and the Underestimation of Variance in Serpent 2. Technical Report VTT-R-00371-14, VTT Technical Research Centre of Finland, 2014.
- [12] VTT Technical Research Centre of Finland. VTT Serpent. <http://montecarlo.vtt.fi/>. Accessed: 2017 April 18.
- [13] E.R Woodcock et al. Techniques used in the GEM code for Monte Carlo neutronics calculations in reactors and other systems of complex geometry. *ANL-7050. Argonne National Laboratory*, 1965.

Appendix A. Pressurized water reactor pin cell data

Table A.4: Cycles/CPU time for the PWR pin cell for the range of t_{wdt} studied. Values in the final column are normalized to the base case without WDT

t_{wdt}	(C/T)	$(C/T)_{norm}$
0.1	42.00	1.00
0.2	40.85	0.97
0.3	39.73	0.95
0.4	32.27	0.77
0.5	31.66	0.75
0.6	31.79	0.76
0.7	31.68	0.75
0.8	31.54	0.75
0.9	31.31	0.75
1.0	31.33	0.75

Appendix B. Fast reactor pin cell data

Appendix C. Homogenous Fuel Element Data

Table A.5: FOM for the PWR pin cell infinite flux, ϕ_∞ , and the FOM normalized to the base case with no WDT, $t_{\text{wdt}} = 0.1$.

t_{wdt}	Fast Group			Thermal Group		
	FOM ($\times 10^3$)	FOM _{norm}	FOM ($\times 10^3$)	FOM _{norm}		
0.1	1248 \pm 5	1.000 \pm 0.000	1293 \pm 11	1.000 \pm 0.000		
0.2	1271 \pm 9	1.018 \pm 0.008	1319 \pm 27	1.020 \pm 0.022		
0.3	1248 \pm 11	0.999 \pm 0.010	1312 \pm 7	1.015 \pm 0.010		
0.4	1292 \pm 6	1.035 \pm 0.006	1321 \pm 9	1.022 \pm 0.011		
0.5	1266 \pm 11	1.014 \pm 0.010	1324 \pm 6	1.024 \pm 0.010		
0.6	1317 \pm 4	1.055 \pm 0.005	1335 \pm 5	1.033 \pm 0.010		
0.7	1309 \pm 5	1.049 \pm 0.006	1320 \pm 8	1.021 \pm 0.011		
0.8	1314 \pm 3	1.052 \pm 0.005	1322 \pm 8	1.023 \pm 0.011		
0.9	1310 \pm 5	1.049 \pm 0.006	1343 \pm 8	1.039 \pm 0.011		
1.0	1304 \pm 14	1.045 \pm 0.012	1358 \pm 13	1.051 \pm 0.013		

Table A.6: FOM for the PWR pin cell fast group infinite total cross-section and the FOM normalized to the base case with no WDT, $t_{\text{wdt}} = 0.1$.

t_{wdt}	Fast Group			Thermal Group		
	FOM ($\times 10^4$)	FOM _{norm}	FOM ($\times 10^4$)	FOM _{norm}		
0.1	1475 \pm 10	1.000 \pm 0.000	811 \pm 3	1.000 \pm 0.000		
0.2	1420 \pm 11	0.963 \pm 0.010	826 \pm 7	1.018 \pm 0.009		
0.3	1380 \pm 12	0.935 \pm 0.010	810 \pm 6	0.999 \pm 0.008		
0.4	1124 \pm 8	0.762 \pm 0.007	824 \pm 6	1.016 \pm 0.008		
0.5	1152 \pm 5	0.781 \pm 0.006	823 \pm 5	1.015 \pm 0.007		
0.6	1190 \pm 4	0.807 \pm 0.006	835 \pm 4	1.030 \pm 0.006		
0.7	1214 \pm 5	0.823 \pm 0.006	854 \pm 9	1.053 \pm 0.012		
0.8	1203 \pm 4	0.816 \pm 0.006	838 \pm 6	1.034 \pm 0.008		
0.9	1221 \pm 7	0.827 \pm 0.007	814 \pm 5	1.003 \pm 0.007		
1.0	1205 \pm 20	0.817 \pm 0.014	866 \pm 13	1.068 \pm 0.017		

Table B.7: Cycles/CPU time for the fast reactor pin cell for the range of t_{wdt} studied. Values in the final column are normalized to the base case without WDT

t_{wdt}	(C/T)	$(C/T)_{\text{norm}}$
0.1	16.92	1.00
0.2	16.58	0.98
0.3	16.01	0.95
0.4	14.96	0.88
0.5	13.81	0.82
0.6	13.05	0.77
0.7	12.51	0.74
0.8	12.55	0.74
0.9	12.51	0.74
1.0	11.32	0.67

Table B.8: FOM for the fast pin cell fast group infinite flux, ϕ_∞ , and total cross-section $\Sigma_{t,\infty}$, and the FOM normalized to the base case with no WDT, $t_{\text{wdt}} = 0.1$.

t_{wdt}	ϕ_∞			$\Sigma_{t,\infty}$		
	FOM ($\times 10^4$)	FOM _{norm}	FOM ($\times 10^4$)	FOM _{norm}		
0.1	141 \pm	1	1.000 \pm 0.000	1141 \pm	8	1.000 \pm 0.000
0.2	146 \pm	1	1.042 \pm 0.013	1136 \pm	7	0.995 \pm 0.009
0.3	164 \pm	2	1.166 \pm 0.018	1250 \pm	13	1.095 \pm 0.014
0.4	171 \pm	2	1.217 \pm 0.015	1301 \pm	20	1.140 \pm 0.019
0.5	171 \pm	1	1.216 \pm 0.013	1292 \pm	12	1.132 \pm 0.013
0.6	188 \pm	2	1.335 \pm 0.018	1367 \pm	24	1.198 \pm 0.023
0.7	184 \pm	4	1.310 \pm 0.028	1237 \pm	19	1.084 \pm 0.018
0.8	180 \pm	2	1.283 \pm 0.019	1341 \pm	14	1.175 \pm 0.014
0.9	177 \pm	2	1.261 \pm 0.020	1332 \pm	15	1.168 \pm 0.015
1.0	160 \pm	1	1.138 \pm 0.013	1212 \pm	12	1.062 \pm 0.013

Table C.9: Cycles/CPU time for the homogenous fuel element for the range of t_{wdt} studied. Values in the final column are normalized to the base case without WDT

t_{wdt}	(C/T)	(C/T) _{norm}
0.1	10.540	1.000
0.2	10.672	1.013
0.3	10.586	1.004
0.4	10.523	0.998
0.5	10.703	1.016
0.6	10.447	0.991
0.7	10.673	1.013
0.8	10.654	1.011
0.9	10.738	1.019
1.0	10.572	1.003

Table C.10: FOM for the homogeneous fuel element infinite flux ϕ_∞ and the FOM normalized to the base case with no WDT, $t_{\text{wdt}} = 0.1$.

t_{wdt}	Fast Group		Thermal Group	
	FOM	FOM_{norm}	FOM	FOM_{norm}
0.1	3065 ± 34	1.000 ± 0.000	7099 ± 95	1.000 ± 0.000
0.2	3085 ± 23	1.006 ± 0.013	6934 ± 49	0.977 ± 0.015
0.3	3088 ± 36	1.007 ± 0.016	6901 ± 40	0.972 ± 0.014
0.4	3254 ± 17	1.062 ± 0.013	7238 ± 41	1.020 ± 0.015
0.5	3180 ± 29	1.037 ± 0.015	7323 ± 28	1.032 ± 0.014
0.6	3065 ± 31	1.000 ± 0.015	7138 ± 86	1.006 ± 0.018
0.7	2999 ± 32	0.978 ± 0.015	7022 ± 34	0.989 ± 0.014
0.8	3232 ± 55	1.054 ± 0.021	7076 ± 86	0.997 ± 0.018
0.9	3058 ± 18	0.998 ± 0.013	7156 ± 38	1.008 ± 0.014
1.0	3162 ± 43	1.031 ± 0.018	7149 ± 43	1.007 ± 0.015

Table C.11: FOM for the homogeneous fuel element infinite total cross-section, $\Sigma_{t,\infty}$, and the FOM normalized to the base case with no WDT, $t_{\text{wdt}} = 0.1$.

t_{wdt}	Fast Group		Thermal Group	
	FOM ($\times 10^3$)	FOM_{norm}	FOM ($\times 10^3$)	FOM_{norm}
0.1	$306 \pm$ 4	1.000 ± 0.000	$1490 \pm$ 14	1.000 ± 0.000
0.2	$311 \pm$ 5	1.017 ± 0.022	$1475 \pm$ 14	0.990 ± 0.013
0.3	$287 \pm$ 4	0.937 ± 0.018	$1485 \pm$ 19	0.996 ± 0.016
0.4	$307 \pm$ 3	1.005 ± 0.017	$1391 \pm$ 8	0.933 ± 0.010
0.5	$325 \pm$ 2	1.062 ± 0.016	$1463 \pm$ 9	0.982 ± 0.011
0.6	$295 \pm$ 5	0.965 ± 0.021	$1409 \pm$ 16	0.945 ± 0.014
0.7	$314 \pm$ 4	1.025 ± 0.019	$1565 \pm$ 27	1.050 ± 0.020
0.8	$326 \pm$ 4	1.066 ± 0.019	$1531 \pm$ 30	1.027 ± 0.022
0.9	$310 \pm$ 2	1.012 ± 0.016	$1489 \pm$ 5	0.999 ± 0.010
1.0	$294 \pm$ 11	0.960 ± 0.038	$1539 \pm$ 12	1.033 ± 0.012